Fiber Optic Refractive Index Distributed Multi-Sensors by Scattering-Level Multiplexing With MgO Nanoparticle-Doped Fibers

Takhmina Ayupova, Madina Shaimerdenova, Sanzhar Korganbayev, Marzhan Sypabekova, Aliya Bekmurzayeva, Wilfried Blanc, Salvador Sales, Guo Tuan, Carlo Molardi, Daniele Tosi

Fiber Optic Refractive Index Distributed Multi-Sensors by Scattering-Level Multiplexing With MgO Nanoparticle-Doped Fibers

Takhmina Ayupova, Madina Shaimerdenova, Sanzhar Korganbayev, Marzhan Sypabekova, Aliya Bekmurzayeva, Wilfried Blanc, Salvador Sales, Tuan Guo, Carlo Molardi, and Daniele Tosi

***Abstract*—In this work, we present the architecture of a multiplexed refractive index (RI) sensing system based on the interrogation of Rayleigh backscattering. The RI sensors are fabricated by fiber wet-etching of a high-scattering MgO nanoparticle-doped fiber, without the need for a reflector or plasmonic element. Interrogation is performed by means of optical backscatter reflectometry (OBR), which allows a detection with a millimeter-level spatial resolution. Multiplexing consists of a simultaneous scan of multiple fibers, achieved by means of scattering-level multiplexing (SLMux) concept, which uses the backscattered power level in each location as a diversity element. The sensors fabricated have sensitivity in the order of 0.473-0.568 nm/RIU (in one sensing point) and have been simultaneously detected together with a distributed temperature sensing element for multi-parameter measurement. An experimental setup has been prepared to demonstrate the capability of each sensing region to operate without cross-talk, while operating multi-fiber detection.**

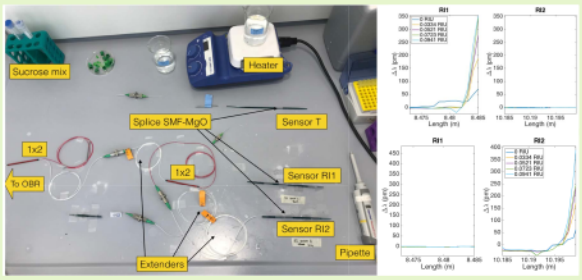

***Index Terms*— Refractive index sensor, optical fiber sensors, distributed sensing, optical backscatter reflectometry, multiplexing.**

I. Introduction

FIBER optic refractive index (RI) sensors are important tools for the detection of the properties of media, and play an important role in environmental science [1], gas detection [2], and biosensors [3]. RI sensors measure the refractive index surrounding an optical fiber device, which is engineered to sense the difference between the inner and external refractive indices. In several applications, these sensors are directly used to detect the RI changes in liquids or gases, in real time. Most notably, RI sensors constitute the platform for fiber-optic biosensors [3]–[5], which are RI sensors functionalized by means of surface chemistry to the selective detection of biological analytes [5].

Traditionally, RI sensors and biosensors are designed by using optical reflectors or transmission filters, which change their spectra as a function of the surrounding RI. A first group of RI sensors makes use of Fiber Bragg Grating (FBG) devices [6]–[10]. While uniform FBGs are not sensitive to RI, it is possible to use an etched FBG (EFBG), in which the fiber diameter is thinned in proximity of the grating introduce a RI sensitivity [6], [7], or a tilted FBG (TFBG), a broadband transmission device in which multiple cladding modes change spectral amplitude and wavelength as a function of the RI [3], [8]. Schemes based on

T. Ayupova, M. Shaimerdenova, and S. Korganbayev are with the Laboratory of Biosensors and Bioinstruments, National Laboratory Astana, 010000 Astana, Kazakhstan (e-mail: takhmina.ayupova@nu.edu.kz; madina.shaimerdenova@nu.edu.kz; skorganbayev@nu.edu.kz).

M. Sypabekova, A. Bekmurzayeva, and D. Tosi are with the Laboratory of Biosensors and Bioinstruments, National Laboratory Astana, 010000 Astana, Kazakhstan, and also with the School of Engineering, Nazarbayev University, 010000 Astana, Kazakhstan (e-mail: msypabekova@nu.edu.kz; abekmurzayeva@nu.edu.kz; daniele.tosi@nu.edu.kz).

W. Blanc is with INPHYNI–CNRS UMR 7010, Université Côte d'Azur, 06108 Nice, France (e-mail: wilfried.blanc@unice.fr).

S. Sales is with the Institute of Telecommunications and Multimedia Applications (iTEAM), Universitat Politècnica de València, 46022 Valencia, Spain (e-mail: ssales@dcom.upv.es).

T. Guo is with the Guangdong Provincial Key Laboratory of Optical Fiber Sensing and Communications, Institute of Photonics Technology, Jinan University, Guangzhou 510632, China (e-mail: tuanguo@jnu.edu.cn).

C. Molardi is with the School of Engineering, Nazarbayev University, 010000 Astana, Kazakhstan (e-mail: carlo.molardi@nu.edu.kz).

long period gratings (LPGs) have also been used for RI detection [9], [10].

Plasmonic devices have also been commonly used as RI sensors [11], [12]; several works have reported in-fiber surface plasmon resonance (SPR) configurations, also assisted by FBGs [13]. SPR sensors are particularly attractive for biosensors, because the metallic thin film that hosts the plasmonic resonance is also an efficient host for bioreceptors [14]. An SPR sensor behaves as a transmission filter, having a shallow spectral dip that shifts with the RI.

Recently, several in-fiber interferometers have been used for RI sensing. Fabry-Perot interferometers (FPI) [15] single-multi-single mode interferometers [16], and in-fiber Sagnac and Fabry-Perot interferometers [17] are attractive thanks to their compact size and good sensitivity. Interferometric sensors have a broadband transmission or reflection spectrum, in which the spectral periodicity changes as a function of the external RI [15]–[17].

When looking at the applications of RI sensors, the previous layouts have three main drawbacks. A first common point is that all the sensors require the micro-fabrication of a sensing device in the fiber. In order to have an in-fiber RI sensor, it is necessary to inscribe an FBG using a phase mask or femtosecond laser [6], [8], or to fabricate an interferometer by means of fiber fusion or CO_2 splicing [15], [16]. Plain SPR sensors are inherently simpler to fabricate as they only require the metallic layer, but the polarization control is needed. A second drawback is that many of the high-sensitivity sensors (SPR, LPG, TFBG) operate in transmission, which makes unpractical to fabricate a probe, since light must be collected after the sensing point. This can be circumvented by adding a gold-tip mirror [3], but it requires an additional element of complexity in the probe. Finally, as many sensors are broadband, it is hard to multiplex sensors using wavelength-division multiplexing (WDM), which is a common feature of FBG sensors [18]. For example, the use of multiplexing technique can lead to a multi-point or multi-parameter sensing network, which can detect temperature(s) in addition to the RI [16].

A first attempt to reduce the fabrication complexity of RI sensors was reported in [19]. In this work, the principle of interrogation is optical backscatter reflectometry (OBR) [20], [21] applied to an etched fiber: rather than detecting a deterministic spectrum, the measurand is the wavelength shift of the Rayleigh backscattering signature due to the change of effective refractive index [19]. Etching, as opposite to the inscription of a reflective element, is a scalable process as it is commonly used in mass production of electronic devices [22].

In this work, we report an OBR-based interrogation of "reflector-less" RI sensors, fabricated as simply etched fiber portions applied to a high-scattering MgO-nanoparticle-doped (MgO-NP) fiber [23]. The etching process introduces a sensitivity to the external RI, while the high backscattering compensates the fiber propagation, scattering, and evanescent losses.

The key feature of the hereby reported sensor is the possibility to multiplex a plurality of sensing point, with an arrangement labeled as scattering-level multiplexing (SLMux) [23]. In the SLMux setup, a single OBR scan interrogates multiple fibers separated by scattering level. In each sensing location, the backscattered power is much larger than the sum of the power scattered by all the other fibers, thus each sensing region can be unambiguously detected.

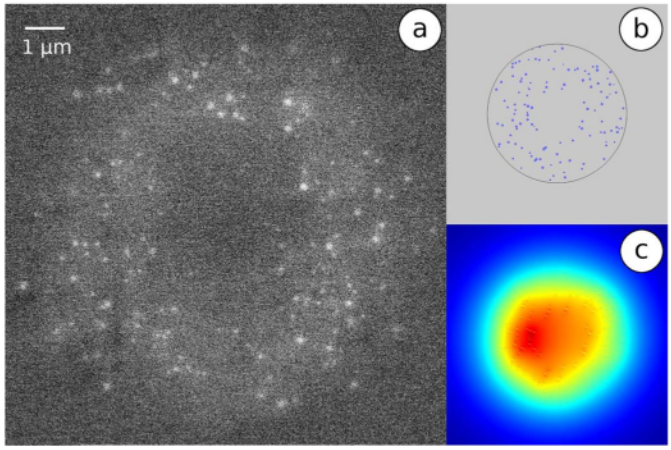

Fig. 1. (a) SEM of the NP-doped fiber cross-section; (b) schematic of the cross-section realization used for the simulation; (c) Modulus of the FM magnetic field.

II. High-Scattering Optical Fiber

The key to enable the principles of SLMux, as explained in [23], is the high backscattering supplied by the special, custom made, MgO-NP doped fiber. The fiber presents the core doped with MgO-based nanoparticles, whose position, size and concentration are random in each section. Precisely, the refractive index of the nanoparticles is estimated to be between 1.53 and 1.65 while the size of the nanoparticles varies between 20 nm and 160 nm, following the distribution shown in [24]. Compared with the fiber used in [19], [23], this one presents bigger nanoparticles, mostly distributed in a ring around the central part of the core, as evident in the scanning electron microscopy (SEM) picture depicted in Fig. 1(a). This results in a larger backscattering, as shown in the next session. The origin of the particles random pattern must be ascribed to the process of fabrication, where a spontaneous phase separation process, between silica substrate and alkaline dopant (Mg), takes place. The result is the formation of two phases: one silica-rich and one MgO-rich in shape of spherical particles. Other than that, the fiber presents typical size of a telecom fiber, i.e. a core diameter of 10 μm and cladding diameter of 125 μm. The core is also co-doped with erbium and germanium, and the difference between the core and cladding refractive indexes is estimated to be $1.7\times10^{-3}-4\times10^{-3}$ [24].

In order to understand the guidance properties of the fiber a set of simulations have been performed, by the use of a full vectorial Finite Element Method (FEM) based software [25]. The cross-section of the simulated fiber, having a random pattern of particles with the same distribution of the real one, is shown in Fig. 1(b). For the simulation the cladding is considered to be composed by pure silica, the refractive index of the core substrate has been chosen equal to 1.4465, while the nanoparticles refractive index has been selected as a random value between 1.53 to 1.65. The simulations operation wavelength is 1550 nm. The presence of the nanoparticle

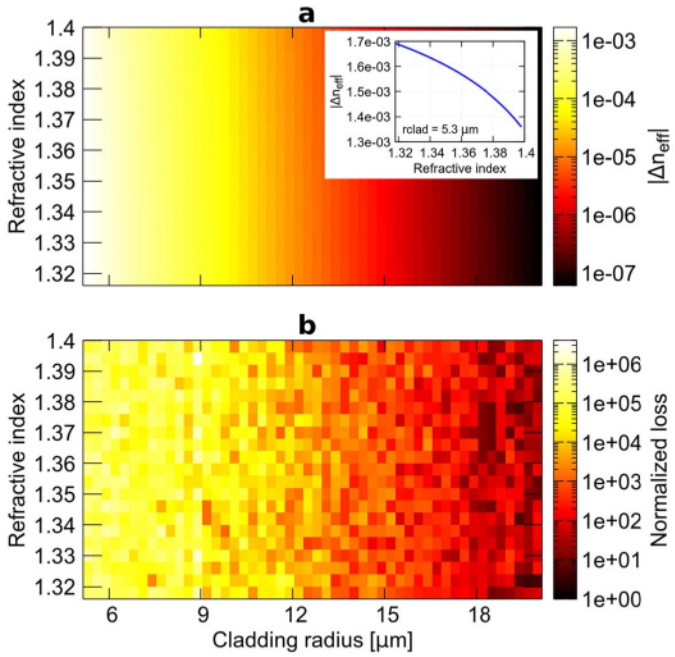

Fig. 2. FEM based simulation of the etched MgO-NP fiber, varying the radius of the cladding and the refractive index of the external solution to analyse. Colour maps of: (a) the differential effective index of the FM with respect the unetched fiber; (b) the propagation loss of the FM, normalized to the loss of the unetched fiber.

increases the confinement of the modes. The fundamental mode (FM), shown in Fig. 1(c), presents a mode field diameter (MFD) of 12.2 μm, slightly higher than a standard SMF-28 telecom fiber.

To determine the performance of the fiber as a refractive index sensor, a second set of numerical simulations have been performed. Two parameters have been varied: the thickness of the etched cladding, going from 5 μm to 20 μm, and the refractive index of the external solution to sense. It has been supposed that the external analyte is based on an aqueous solution of sucrose with concentration varying from 0% to 40 %. This is equivalent to a refractive index varying between 1.334 and 1.400 [26]. Results are shown in Fig. 2.

In the colour map, depicted in Fig. 2(a), it is possible to appreciate the variation of the differential effective index (Δn_{eff}) of the FM, defined as the difference between the effective index of the etched fiber surrounded by a solution of sucrose and the effective index of the pristine fiber. The trend of the FM effective index is to reduce along with the decrease the cladding thickness, since the evanescent field of the FM starts to interact with the analyte, which presents a lower refractive index with respect to the cladding, made of pure silica. The dependence of the FM differential effective index on the cladding radius shows a typical negative exponential trend, as shown in [26]. When the cladding is mostly removed, the Δn_{eff} is in the order of 1×10^{-3}, moreover the guidance properties of the fundamental mode are strongly influenced by the refractive index of the analyte. As shown in the inset of Fig. 2(a), when the cladding radius is equal of 5.3 μm the variation of the Δn_{eff} is in the order of 1×10^{-4}, showing an average relative sensitivity of 4.4×10^{-3} RIU/Δn_{eff}. Thus, a change in RI surrounding the etched fiber results in a change of

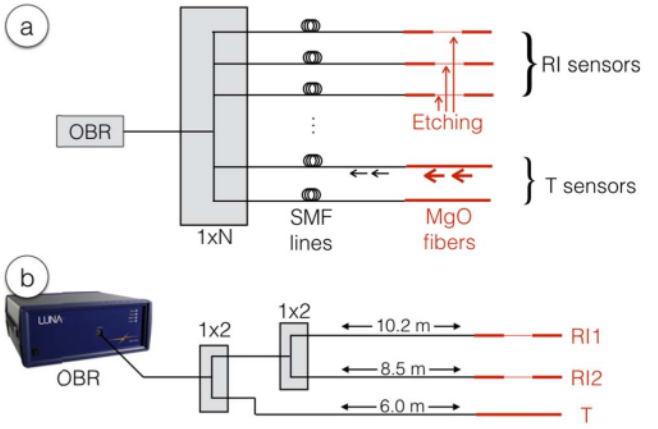

Fig. 3. Schematic of the SLMux concept for RI and physical sensing. (a) Generic scheme for a N-channel system, made of SMF cables serving as in-line extenders, and a network of distributed sensors based on MgO-NP fibers which are etched for RI sensing, or unetched for physical sensing. (b) Schematic of the setup implemented in this work, with a network of 1x2 splitters, two RI sensors and one temperature sensors, with cables having length of 10.2 m, 8.5 m, and 6.0 m respectively (measured from the OBR connector).

the effective refractive index, which itself causes a shift of the Rayleigh scattering signatures in the frequency domain [19].

While the behaviour of the effective index is related to the spatial accuracy of the distributed sensors, a larger importance is embedded in the behaviour of the propagation loss, which are strictly correlated to the backscattering of the fiber. In the colour map of Fig. 2(b) the normalized propagation loss, defined as the ratio between the propagation loss of the etched fiber and the propagation loss of the pristine fiber, is depicted. It is possible to see that the propagation loss largely increases with the decrease of the cladding radius. Although the reduction of the cladding thickness increases the mode confinement, the propagation loss becomes more than 1×10^5 times larger when the cladding radius is less than 10 μm. The presence of the residual cladding ring can induce local resonances, with the effect of decreasing the loss for a specific value of the analyte refractive index, as shown by the darker dots in the high loss region of Fig. 2(b).

III. Experimental Setup

The experimental setup is sketched in Fig. 3 and shown photographically in Fig. 4. The upper chart of Fig. 3 shows a generic implementation of a SLMux concept for a N-channel sensing, whereas each sensing region can serve as either a physical sensor (strain or temperature) with a bare MgO fiber, or as a RI sensor by etching the fiber in the corresponding sensing region.

A network of SMF (single-mode fiber) extenders is used to perform the delay line function: by choosing the length of each SMF it is possible to set a different position on the length axis z for each sensing fiber. We can then convert the overall signature pattern (i.e. the individual spectra of Rayleigh backscattering in each fiber section) into the wavelength shift estimated in each sensing section: this occurs because the scattering level in each MgO-NP is much higher than the combination of all the other SMF fibers in the corresponding location [23], [26].

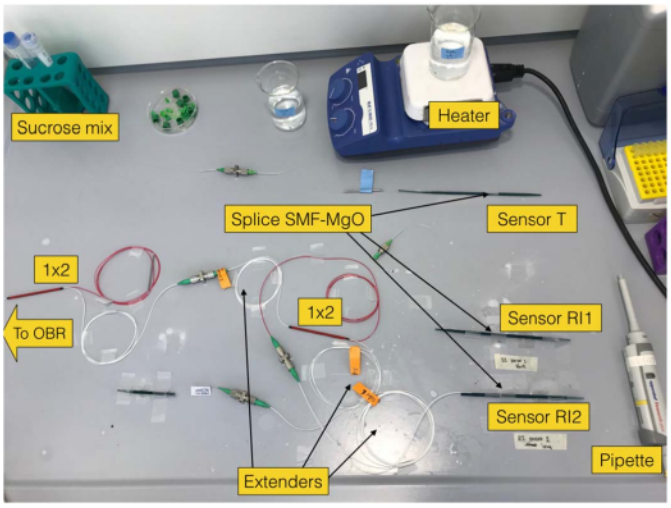

Fig. 4. Photograph of the experimental SLMux setup, showing the optical circuitry, the sensors, and the inner connectors. RI has been changed pipetting a water/sucrose mixture, while temperature has been increased with a heater.

This approach is here labelled SLMux, because it is a spatial multiplexing concept in which the diversity is in the scattering level differential and allows interrogating multiple fiber sensors. In each sensing section, the system behaves as a distributed sensor with spatial resolution $\Delta z = c \,/\, (2\, n_{eff}\, \Delta f) = 9.6\ \mu$m ($c$ = speed of light, n_{eff} = effective refractive index of main mode propagating in the fiber, Δf = frequency range of the OBR swept laser) [20]. In comparison to multicore fiber-based spatial division multiplexing [28], this architecture is attractive as the sensors are hosted in multiple fibers, which can reach different locations rather than having all sensors stacked in a single fiber. We consider also that the length of the SMF spools separating the MgO-NP sensors is chosen by design, in order to avoid the overlap of each sensing zone, making the system scalable.

The bottom chart, Fig. 3(b) shows the setup that has been implemented in this work, which demonstrates the SLMux. This setup is based on 3 sensors, two performing RI sensing (labelled RI1 and RI2) and consisting of an etched fiber, and one performing temperature sensing (labelled T) and consisting of a bare MgO-NP fiber.

The interrogator is an OBR system based on swept-laser interferometry (Luna Inc., OBR4600) [21]. The OBR operates on the 1525.0-1610.5 range with 9.6 μm spatial resolution; spot size and distributed sensing options have been enabled for the measurement. The OBR speed is 3 Hz, and gage length 1 mm. The OBR detects the spectral signals of the Rayleigh backscattering in each portion of the fiber, i.e. the so-called signatures; by measuring the correlation between the signature acquired at the measurement start and the current signature, it is possible to measure the instantaneous wavelength shift [20]. A network of two 1×2 splitters is used to obtain 3 separate channels, each having a different lead-out length that identifies each sensor unambiguously. The MgO-NP fibers are spliced to SMF fibers by a standard splicer (Fujikura 12-S, SMF-SMF splice mode).

The scattering traces are reported in Fig. 5. We note that each sensor occupies a different portion of the overall trace,

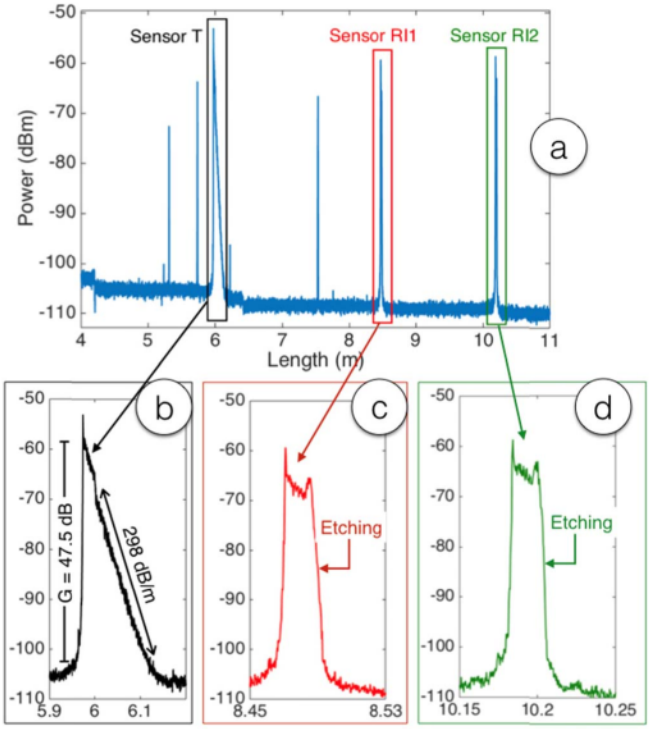

Fig. 5. Backscattering traces for the SLMux configuration. (a) Original trace, when all the 3 sensors are connected. (b-d) The insets show the portion of trace occupied by each sensor T, RI1, and RI2 respectively. Sensors are placed in air for this measurement; hence exhibiting the highest propagation loss.

according to the length of the lead-in SMF cable (measured from the source). The RI sensors are set at longer distance, and appear as a scattering rise, followed by a drop corresponding to the scattering-induced losses, and a subsequent drop (1.0 dB/mm and 4.2 dB/mm for sensors RI1 and RI2 when placed in air) which merges scattering and propagation losses. The temperature sensor appears as a triangular shape in terms of scattering trace: the fiber has a scattering gain of 47.5 dB with respect to the SMF, followed by a subsequent loss of 298 dB/m. The several peaks appearing on Fig. 5(a) in the other regions are due to the several FC/APC connectors used in the setup.

IV. Sensors Fabrication and Characterization

The RI sensors have been fabricated individually, prior to arranging the SLMux setup; thus, the length coordinate visualized in this section has an offset with respect to Fig. 5 and the next section.

RI sensors have been fabricated by wet etching in hydrofluoric acid (48% for 30 minutes, followed by 24% for 23 minutes). Fig. 6 shows the scattering trace as a function of time elapsed in etching solution, for RI1 sensor. It is possible to see that, after around 46 minutes from the initial stage, as the fiber cladding gets thinned the amount of evanescent field increases, causing additional losses that are well visible in the portion of fiber following the etching zone. At the end of the etching process, the loss differential between the initial fiber and the etched fiber is 31 dB. A similar result is achieved for RI2. The estimated fiber diameter after etching is around 14 μm.

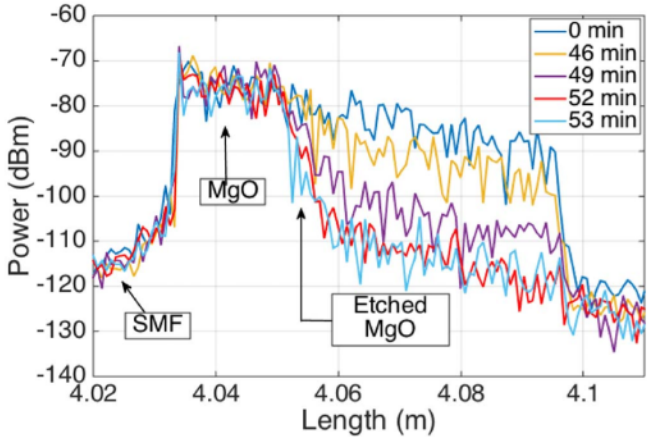

Fig. 6. Backscattering traces for RI1 sensor during the HF etching process, at different etching times.

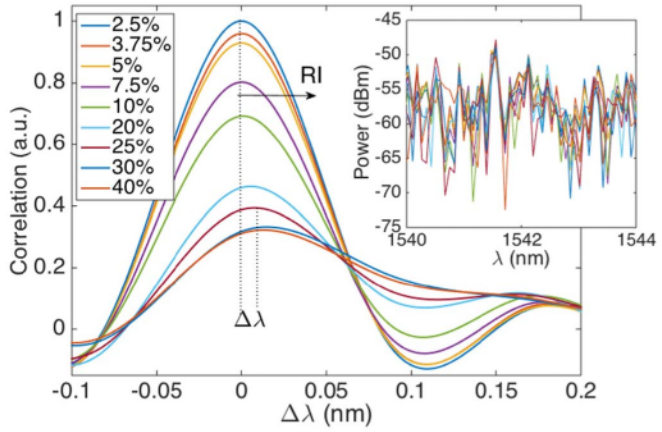

Fig. 7. Mutual correlation (normalized between to a value of 1) between the reference signature (in water) and the signatures acquired at different levels of sucrose (2.5% to 40%) for sensor RI1. The inset shows a portion of the signatures, reporting the power as a function of wavelength.

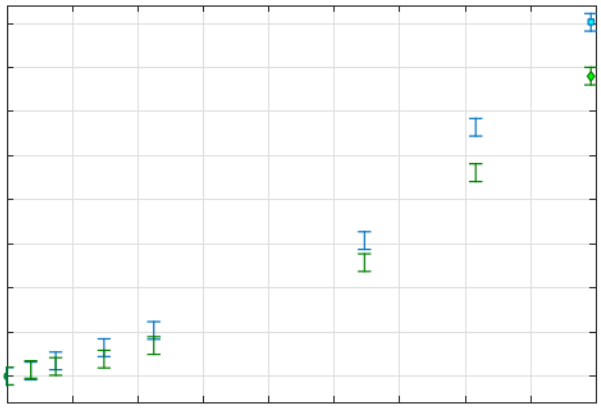

Fig. 8. Calibration functions of 2 sensing points within the range of RI1 and RI2 sensors; the curves show the wavelength shift as a function of RIU change (baseline RI value of 1.3366). A linear fit in the first part of the curve is applied to estimate the sensitivity. Error bars show the uncertainty of the OBR.

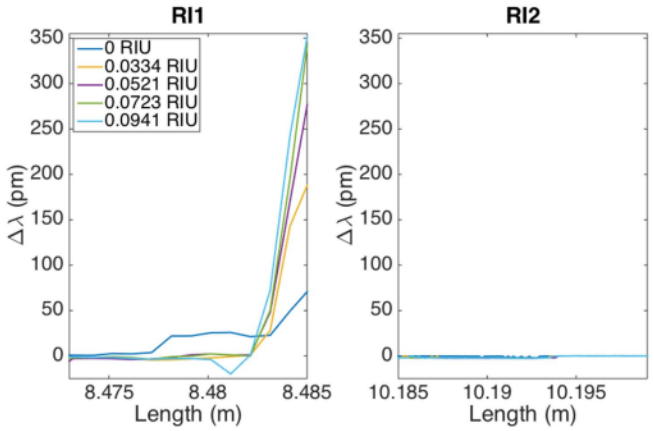

Fig. 9. Wavelength shift for RI1 (8.473 – 8.485 m) and RI2 (10.185 – 10.199 m) sensing regions, when the refractive index of sensor RI1 is changed from 0 to 0.0941 RIU and RI2 is at a constant refractive index.

The operation of the RI sensor is shown in Fig. 7. At each length, evaluated within the RI1 sensing points, we acquire the signature (that corresponds to the backscattered power as a function of wavelength λ), which is shown in the inset of the figure. By comparing the signature in reference condition, with the signatures acquired at different RI values, we observe that the correlation shifts in wavelength, and reduces in amplitude.

In order to measure this relationship, we performed a measurement similar to [19], immersing the sensor in a mixture of water and sucrose, with sucrose values 2.5% to 40% that progressively increase the RI. We therefore compute the mutual correlation function, for each value of wavelength shift $\Delta\lambda$, estimating then the correlation peak by using the spline peak tracking method as in [29].

The calibration of the sensors is shown in Fig. 8, which reports the sensitivity, evaluated as wavelength shift for each change of RI. As in [19], the sensitivity is approximately linear for lower values of RI, and subsequently increases as the RI change is larger than 0.027 RIU. By applying a linear fit in the first part of the curve, we can estimate the sensitivity as 0.568 nm/RIU for RI1 and 0.473 nm/RIU for RI2. Given that the resolution of wavelength detection is ≈0.3 pm [29], we therefore estimate the detection limit at 5.2×10^{-4} RIU for RI1 and 6.3×10^{-4} RIU for RI2.

We remark that, given the distributed nature of the sensor, these values do not represent the sensitivity of the RI1-2 sensors, but rather the sensitivity of a single point within the active region; the multiple points in the etched region have a sensitivity that depends on the local thickness of the fiber. In this case, the sensitivity is evaluated at the center of the sensing region.

V. Multiplexing Analysis

The key approach proposed in this work is to evaluate the possibility to multiplex different RI sensors on different fibers, while maintaining distributed sensing on each sensing region; in this section, we report the results of a multiplexing analysis, in which the refractive index at RI1 and RI2 and the temperature at T are independently varied, thus estimating sensor crosstalk.

Experiments have been carried out with the setup shown in Fig. 4, using a pipette to change the RI of each sensor by changing the sucrose percentage, and using a heating place (IKA C-Mag) to change the temperature. The MgO-NP fiber, calibrated as in [23], has a temperature coefficient of 11.9 pm/°C. For each experiment hereby reported, we show the difference in response between the sensor exposed to the measurand, and another sensor standing at reference value.

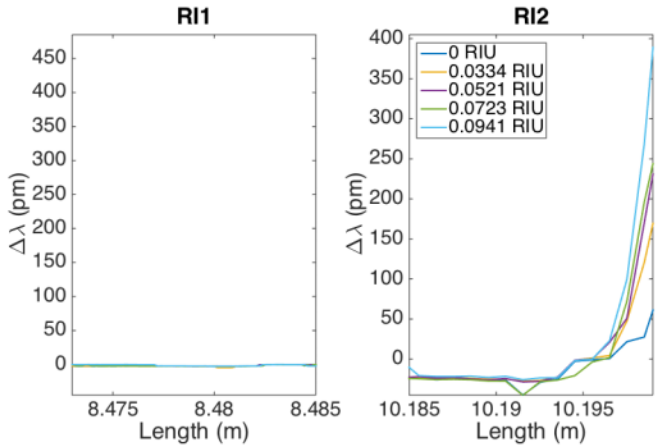

Fig. 10. Wavelength shift for RI1 (8.473 – 8.485 m) and RI2 (10.185 – 10.199 m) sensing regions, when the refractive index of sensor RI2 is changed from 0 to 0.0941 RIU and RI1 is at a constant refractive index.

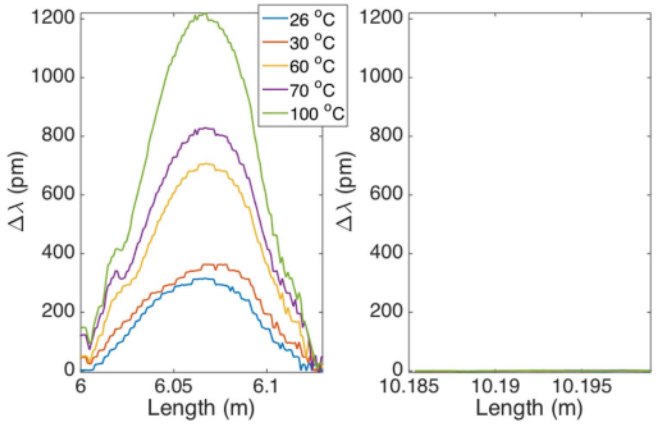

Fig. 11. Wavelength shift for T (6.00 – 6.13 m) and RI2 (10.185 – 10.199 m) sensing regions, when the temperature of T sensor is changed through heating and the RI of sensor RI2 is held constant.

Fig. 9 shows the wavelength shift of RI1 and RI2 changes, when RI1 is exposed to multiple RI values and RI2 is at reference condition. Similarly, Fig. 10 we show he counterpart measure, when the RI of sensor RI2 is varied and RI1 is held at constant RI value.

We identify the sensor RI1 with the length of 8.477 – 8.485 m, while prior to this length, the fiber is unetched and therefore is not exposed to RI sensitivity. Similarly, the sensor RI2 ranges within 10.191 – 10.199 m length, both having 8 mm length. From the charts, we observe the correct functioning of the SLMux: while the sensing region of one sensor changes in response to the RI change, the other sensor does not respond. In the first case, the maximum wavelength shift observed is 349 pm, while in the second case it is 398 pm; conversely, the sensors held at the reference condition exhibit a much inferior wavelength shift (2.5 pm for Fig. 9, 4.4 pm for Fig. 10).

We also observe that the maximum sensitivity of both sensors is observed at the tip of the fiber, whereas the sensitivity calculated in Fig. 8 has been accounted at the center of the sensing region. This is mainly due to the fact that the etched fiber has a conical shape with the tip thinner than the tail as in [26], thus we expect a larger shift on the thinner tip; experimentally, though, sensing points closer to the tip are more subjected to power fluctuations, so real-time sensing is more robust in inner portion of the etched fiber.

Finally, in order to evaluate the possibility to multiplex RI and temperature sensing, we performed an experiment in which the T sensor (6.00 - 6.13 m) is exposed to a temperature change and the RI sensors are held constant. The result is shown in Fig. 11, which reports the wavelength shift for RI2 and T sensors when temperature of the oven changes. For this experiment, the temperature of the heating plate is varied between 26 °C and 100 °C, and the T fiber is placed in proximity of the heating plate, such that only the central part of the sensing region is exposed to the maximum change of temperature.

We observe that the sensor T is, as we expect, exposed to a change of temperature and exhibits a non-uniform patter in the center, that corresponds to the heating distribution. The peak wavelength shift is 1201 pm. On the other hand the sensor RI2 does not exhibit a wavelength change, with the maximum variation equal to 3.6 pm.

Overall, we can conclude that the SLMux concept is demonstrated: when one measurand is varied, only the correspondent sensor responds, while the other sensors exhibit no sensitive change, and thus no cross-sensitivity. The sensor drift however is larger than the 0.3 pm accuracy of detection, mainly due to the fact that when the SLMux setup is connected, the signatures of the SMF fiber in correspondence of each MgO-NP fiber act as an additional noise. This effect can be mitigated by choosing the sensing point with the highest sensitivity.

VI. Conclusions

This work proposes and experimentally demonstrates a SLMux configuration, which allows expanding OBR inline sensing, a concept applied to a single optical fiber, to a multi-fiber sensing network that can interrogate both RI sensors and physical sensors (temperature or strain).

The concept requires a high-scattering fiber, which is capable of sustaining the propagation and scattering losses and, at the same time, rise the scattering level of each sensing region such that the signature can be unambiguously detected. This approach is verified in this work, as the cross-talk is limited and the correlation of each signature can detect each signature.

This method is intriguing for RI sensing, and potentially for biosensing, as the fabrication of each sensing point is minimalistic; we label this concept as “reflector-less” sensing, as we can simply etch a fiber to turn it into a RI sensor, without the need of a grating, interferometer, plasmonic device. This approach effectively extends spatial division multiplexing on multicore fibers, because we can stack each sensor on a physically different sensing fiber (positioned at different location) rather than having multiple sensors on the same fiber.

In this work, the concept is demonstrated and the sensitivity is in the range of 0.473 - 0.568 nm/RIU, a value lower than several other approaches, but achieved maintaining the distributed sensing feature, working on multiple sensing fibers, and still capable of working below the 10^{-3} RIU detection limit.

The margins of improvements are huge, both in terms of fiber design (including scattering control and sensitivity to the external RI by controlling the MgO nanoparticles) and by etching at a deeper penetration, closer to the core. For this demonstration, we worked on a relatively shallow etching (around 13 μm fiber diameter), which still preserves a sufficient tensile strength of the fiber for performing experimental analysis. Clearly, increasing the etching allows an expansion of the sensitivity [19], although it would also cause higher losses, which need to be sustained by the high scattering of the fiber.

Future work will revolve on optimizing the fiber design and layout of the interrogator, and on functionalizing the MgO-NP fiber for biosensing.

References

[1] K. Yüksel, "Optical fiber sensor system for remote and multi-point refractive index measurement," *Sens. Actuators A, Phys.*, vol. 250, pp. 29–34, Oct. 2016.

[2] M. Quan, J. Tian, and Y. Yao, "Ultra-high sensitivity Fabry–Perot interferometer gas refractive index fiber sensor based on photonic crystal fiber and Vernier effect," *Opt. Lett.*, vol. 40, no. 21, pp. 4891–4894, 2015.

[3] T. Guo, F. Liu, B.-O. Guan, and J. Albert, "Tilted fiber grating mechanical and biochemical sensors," *Opt. Laser Technol.*, vol. 78, pp. 19–33, Apr. 2016.

[4] A. Leung, P. M. Shankar, and R. Mutharasan, "A review of fiber-optic biosensors," *Sens. Actuators B, Chem.*, vol. 125, no. 2, pp. 688–703, 2007.

[5] O. S. Wolfbeis, "Fiber-optic chemical sensors and biosensors," *Anal. Chem.*, vol. 80, no. 12, pp. 4269–4283, 2008.

[6] A. Iadicicco, A. Cusano, S. Campopiano, A. Cutolo, and M. Giordano, "Thinned fiber Bragg gratings as refractive index sensors," *IEEE Sensors J.*, vol. 5, no. 6, pp. 1288–1295, Dec. 2005.

[7] A. Bekmurzayeva *et al.*, "Etched fiber Bragg grating biosensor functionalized with aptamers for detection of thrombin," *Sensors*, vol. 18, no. 12, p. 4298, Dec. 2018.

[8] B. Jiang *et al.*, "Label-free glucose biosensor based on enzymatic graphene oxide-functionalized tilted fiber grating," *Sens. Actuators B, Chem*, vol. 254, pp. 1033–1039, Jan. 2018.

[9] F. Esposito, L. Sansone, C. Taddei, S. Campopiano, M. Giordano, and A. Iadicicco, "Ultrasensitive biosensor based on long period grating coated with polycarbonate-graphene oxide multilayer," *Sens. Actuators B, Chem.*, vol. 274, pp. 517–526, Nov. 2018.

[10] A. Iadicicco, R. Ranjan, F. Esposito, and S. Campopiano, "Arc-induced long period gratings in polarization-maintaining PANDA fiber," *IEEE Photon. Technol. Lett.*, vol. 28, no. 18, pp. 1533–1536, Sep. 15, 2017.

[11] A. K. Sharma, R. Jha, and B. D. Gupta, "Fiber-optic sensors based on surface plasmon resonance: A comprehensive review," *IEEE Sensors J.*, vol. 7, no. 8, pp. 1118–1129, Aug. 2007.

[12] C. Fallauto, Y. Liu, G. Perrone, and A. Vallan, "Compensated surface plasmon resonance sensor for long-term monitoring applications," *IEEE Trans. Instrum. Meas.*, vol. 63, no. 5, pp. 1287–1292, May 2014.

[13] C. Caucheteur, Y. Shevchenko, L.-Y. Shao, M. Wuilpart, and J. Albert, "High resolution interrogation of tilted fiber grating SPR sensors from polarization properties measurement," *Opt. Express*, vol. 19, no. 2, pp. 1656–1664, 2011.

[14] X. D. Hoa, A. G. Kirk, and M. Tabrizian, "Enhanced SPR response from patterned immobilization of surface bioreceptors on nano-gratings," *Biosens. Bioelectron.*, vol. 24, no. 10, pp. 3043–3048, Jun. 2009.

[15] Y. Zheng *et al.*, "Miniature pH optical fiber sensor based on Fabry–Perot interferometer," *IEEE J. Sel. Topics Quant. Electron.*, vol. 22, no. 2, Apr. 2016, Art. no. 5600205.

[16] L. Hou, X. Zhang, J. Yang, J. Kang, and L. Ran, "Simultaneous measurement of refractive index and temperature based on half-tapered SMS fiber structure with fringe-visibility difference demodulation method," *Opt. Commun.*, vol. 433, pp. 252–255, Feb. 2019.

[17] S. Gao *et al.*, "High-sensitivity DNA biosensor based on microfiber Sagnac interferometer," *Opt. Express*, vol. 25, no. 12, pp. 13305–13313, 2017.

[18] A. Kersey *et al.*, "Fiber grating sensors," *J. Lightw. Technol.*, vol. 15, no. 8, pp. 1442–1463, Aug. 1997.

[19] M. Sypabekova *et al.*, "Fiber optic refractive index sensors through spectral detection of Rayleigh backscattering in a chemically etched MgO-based nanoparticle-doped fiber," *Opt. Lett.*, vol. 43, no. 24, pp. 5945–5948, 2018.

[20] M. E. Froggatt and J. Moore, "High-spatial-resolution distributed strain measurement in optical fiber with Rayleigh scatter," *Appl. Opt.*, vol. 37, no. 10, pp. 1735–1740, 1998.

[21] B. J. Soller, D. K. Gifford, M. S. Wolfe, and M. E. Froggatt, "High resolution optical frequency domain reflectometry for characterization of components and assemblies," *Opt. Express*, vol. 13, no. 2, pp. 666–674, 2005.

[22] G. A. C. M. Spierings, "Wet chemical etching of silicate glasses in hydrofluoric acid based solutions," *J. Mater. Sci.*, vol. 28, no. 23, pp. 6261–6273, 1993.

[23] A. Beisenova *et al.*, "Multi-fiber distributed thermal profiling of minimally invasive thermal ablation with scattering-level multiplexing in MgO-doped fibers," *Biomed. Opt. Express*, vol. 10, no. 3, pp. 1282–1296, 2019.

[24] W. Blanc *et al.*, "Fabrication of rare earth-doped transparent glass ceramic optical fibers by modified chemical vapor deposition," *J. Amer. Ceram. Soc.*, vol. 94, no. 8, pp. 2315–2318, Aug. 2011.

[25] S. Selleri, L. Vincetti, A. Cucinotta, and M. Zoboli, "Complex FEM modal solver of optical waveguides with PML boundary conditions," *Opt. Quant. Electron.*, vol. 33, nos. 4–5, pp. 359–371, Apr. 2001.

[26] T. Ayupova *et al.*, "Wavelet-based demodulation of Multimode etched fiber Bragg grating refractive index sensor," *MDPI Sensors*, vol. 19, no. 1, p. 39, Dec. 2018.

[27] A. Yan *et al.*, "Distributed optical fiber sensors with Ultrafast laser enhanced rayleigh backscattering profiles for real-time monitoring of solid oxide fuel cell operations," *Sci. Rep.*, vol. 7, no. 1, p. 9360, Aug. 2017.

[28] I. Gasulla, D. Barrera, J. Hervas, and S. Sales, "Spatial division multiplexed microwave signal processing by selective grating inscription in homogeneous multicore fibers," *Sci. Rep.*, vol. 7, Jan. 2017, Art. no. 041727.

[29] D. Tosi, "Review and analysis of peak tracking techniques for fiber Bragg grating sensors," *Sensors*, vol. 17, no. 10, p. 2368, Oct. 2017.